Supplement for "Molecular simulation of hybrid polymer nanocomposites with organic nanodimers and inorganic nanorods: from structure and dynamics to viscosity"

Adri Escañuela-Copado,[1] Alberto Martín-Molina,[1,2] and Alessandro Patti[1,2,3,a)]

[1)] *Biocolloid and Fluid Physics Group, Department of Applied Physics, Universidad de Granada, 18071 Granada, Spain*

[2)] *Carlos I Institute of Theoretical and Computational Physics, 18071 Granada, Spain*

[3)] *Department of Chemical Engineering, The University of Manchester, Manchester M13 9PL, United Kingdom*

[a)] Electronic mail: apatti@ugr.es

S1. DETAILS OF THE MODEL

TABLE S1: Interactions, in units of ε_0, for the non-bonded interaction potential.[a]

Bead i	M_1	M_1	M_2	M_1	M_1	M_2	M_2	M	M	M	ND_1	ND_1	ND_2	NR	NR	NR	NR
Bead j	M_1	M_2	M_2	$ND_J^{(1)}$	$ND_J^{(2)}$	$ND_J^{(1)}$	$ND_J^{(2)}$	ND_1	ND_2	NR	ND_1	ND_2	ND_2	ND_J	ND_1	ND_2	NR
$\varepsilon_{ij}/\varepsilon_0$	1.0	2.5	1.0	0.1	1.0	1.0	0.1	1.0	0.1	1.0	1.0	1.0	1.0	1.0	1.0	1.0	2.5

[a] M_1 is the homopolymer bead as well as one of the two block-copolymer beads, the other being M_2. M is used for both polymer beads indistinctly. ND_1 and ND_2 are the beads of the homogeneous nanodimers. The upperscript in $ND_J^{(1)}$ and $ND_J^{(2)}$ distinguishes between the beads of each Janus nanodimer when such distinction is needed. NR represents the generic beads of nanorods.

The non-bonded interaction energies between each bead in our coarse-grained simulation are listed in Tab. S1. As stated in Tab. I of the main text, ND-PNCs contain 40 NDs; using the coarse-grained bead masses given at Tab. S2, that corresponds to exactly 5.027 wt.% concentration. NR-PNCs contain 66 NRs, resulting in a 5.042 wt.% concentration. The concentration of nanoparticles in ND_k/NR-PNCs, which includes 40 NRs and 40 NDs, is 7.843 wt.%. The densities of monomers and NDs are fixed to the density of a polyethylene bead,[1] of mass $m_M = 44.07$ g mol^{-1} and diameter $\sigma_M = 0.42$ nm. Consequently, NDs are considered organic particles, as is the polymer. The density of NRs is exactly 3.33 times the polymer's bulk density ($\rho_{\mathrm{org}} = 851$ kg m^{-3}, as reported by Everaers[1]), resulting in $\rho_{\mathrm{NR}} = 2833.83$ kg m^{-3}, which corresponds to metallic or silica-like NRs.

The bonding distance between lobes of a ND shown in Tab. S2 is obtained using the criteria found in the work of J.J. Burgos-Mármol and A. Patti.[2] We set exclusions between the two lobes to prevent the repulsive non-bonded interaction from disrupting the bonding distance. For NRs, the bonding distance is related to their rugosity, which is set to $\xi = 0.1$, or 10 %. The bonding distance between monomers inside the polymer chain can be determined numerically by finding the minimum in a combination of the WCA and FENE potentials.

In our whole system, bead movement is stochastic, following Langevin dynamics. It is expressed in the following equations of motion:

$$m_i \frac{\mathrm{d}^2 \mathbf{r}_i}{\mathrm{d}t^2} = \mathbf{F}_i - \zeta_i m_i \frac{\mathrm{d}\mathbf{r}_i}{\mathrm{d}t} + \mathbf{N}_i \,. \tag{1}$$

$\mathbf{F}_i = -\boldsymbol{\nabla} V_i^{\text{total}}$ represents the conservative forces acting on particle i, driven by the total potential that it is subject to. $\mathbf{N}_i$ is a noise process dependent on temperature T, which can be interpreted as a thermal force. This noise is described by the autocorrelator at two different times t_1 and t_2 as $\langle \mathbf{N}_i(t_1)\mathbf{N}_j(t_2)\rangle = 2\zeta_i m_i k_{\text{B}} T \delta(t_1 - t_2)\delta_{ij}$ where $\delta(t')$ a Dirac delta for a given t' and δ_{ij} a Kronecker delta. The parameter ζ_i of the thermal noise introduces velocity-dependent term in the equation of motion, Eq. (1), serving as a friction parameter. We derive the friction parameter for each bead using the self-interaction energy of each bead ε_{ii} by first defining a self-relaxation time τ_i,

$$\tau_i \equiv \sigma_i \sqrt{m_i/\varepsilon_{ii}}\,, \qquad \zeta_i \equiv \beta_i m_i/\tau_i\,, \tag{2}$$

with $\beta_i = 0.5$ for polymers, following the Kremer-Grest model,[3,4] and $\beta_i = 1$ for the rest of the particles. The values of ζ_i for each bead are shown in Tab. S2.

TABLE S2: Parameters employed to construct each coarse-grained bead of the PNCs.[a,b]

	σ_i (nm)	m_i (g mol^{-1})	ζ_i (g mol^{-1} ps^{-1})
M	0.42	44.0700	12.433
ND	1.26	1166.3231	42.641
NR	0.63	709.0374, 2 mass sites	26.284, 8 virtual sites

	Δ_{ij} (nm)
M_1-M_1 or M_2-M_2	0.40838, FENE+WCA
M_1-M_2	0.41961, FENE+WCA
ND$^{(1)}$-ND$^{(2)}$	1.05798, harmonic
NR$^{(i)}$-NR$^{(j)}$	0.36000, constrained

[a] M is used for both polymer beads indistinctly, ND represents a nanodimer and NR a nanorod.

[b] σ_i denotes diameter, m_i is the mass of the bead, ζ_i is the friction parameter and Δ_{ij} denotes bonding distance between consecutive beads.

S2. NANOROD CRYSTAL FORMATION

In various simulations of PNCs that included NRs, we observed their eventual nucleation into crystal configurations driven by the depletion interaction. The WCA potential exerted a repulsion between NRs and monomers, prompting the NRs to assemble into these structures. We can see this evolution in the various snapshots of Fig. S1. This assembly minimizes their surface contact and enhances the free volume for polymer chains, thereby increasing the overall entropy of the system by allowing a greater number of configurations that the polymer chains can explore.

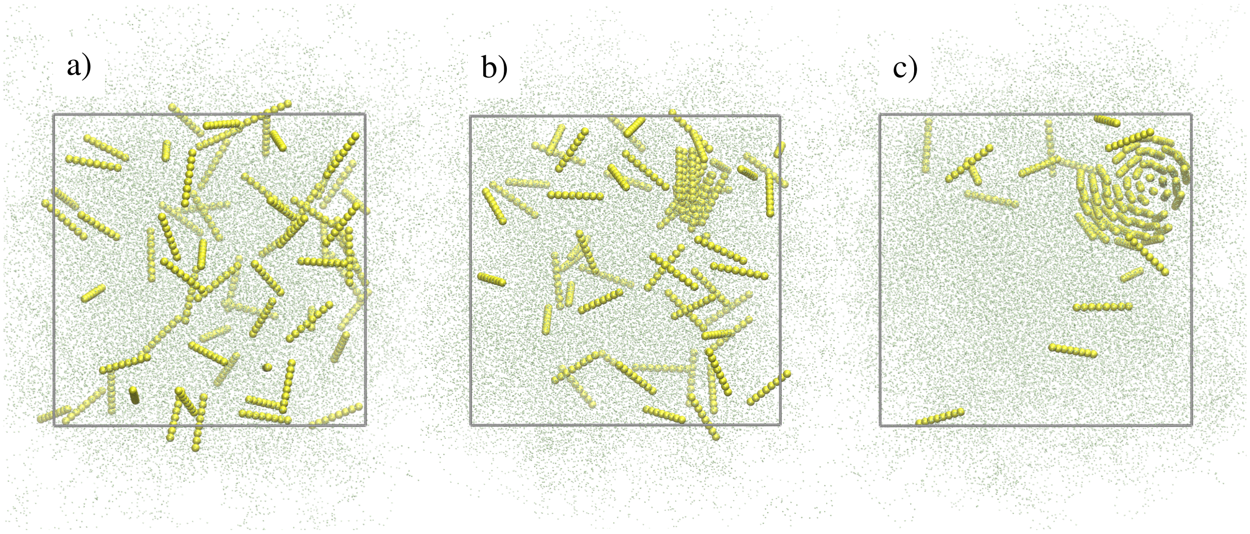

FIG. S1: Three snapshots showing the nucleation of a crystal in the upper right corner of an NR-HPNC.

In order to avoid these defects, we switched from a WCA potential, which is a purely repulsive Lennard-Jones potential, to a standard Lennard-Jones potential. This change allows the NRs to feel an attraction with the monomers at a certain distance, creating an effect similar to a soft polymer grafting around them. This acts as if the NRs surrounded by polymer are attracted to the melt, stabilizing the system and preventing the formation of defects.

S3. RADIAL DISTRIBUTION FUNCTIONS

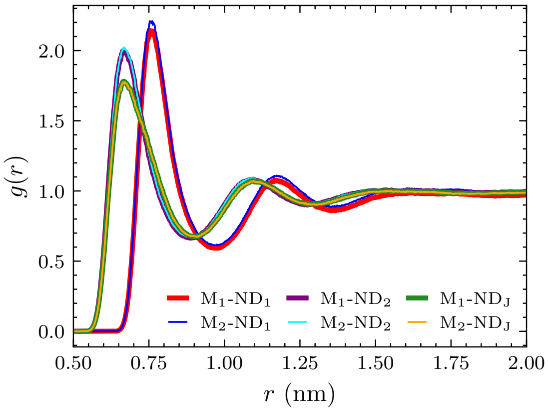

FIG. S2: RDFs of the monomers M_1 and M_2 centered on the NDs' centers of mass. To highlight and distinguish between overlapping curves, different colors and line widths are used, as indicated in the legend.

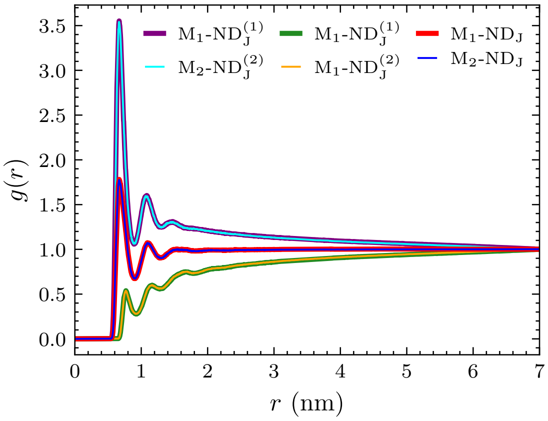

FIG. S3: RDFs of the monomers M_1 and M_2 centered on the Janus NDs' centers of mass. To highlight and distinguish between overlapping curves, different colors and line widths are used, as indicated in the legend.

We start discussing the RDFs of monomers around NDs. In Fig. S2, we check that the monomer distribution around NDs' centers of mass is indifferent of the monomer type. Figure S3 illustrates that, due to the Janus ND dual affinity to the different polymeric blocks, the $ND_J^{(1)}$ lobe tends to be surrounded by M_1 monomers, since their radial distribution is always greater than 1, $g(r) > 1$. The same happens for $ND_J^{(2)}$ lobes and M_2 monomers, and with the same intensity, as the two curves overlap. In fact, one can check on Tab. S1

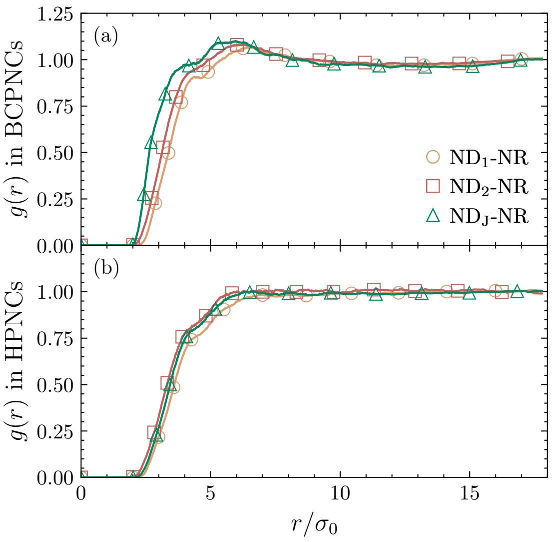

FIG. S4: RDFs between the NDs' and NRs' centers of mass in ND_k/NR-BCPNCs (top frame) and ND_k/NR-HPNCs (bottom frame). Solid lines are guides for the eye.

that these interactions are of the same strength, a value of $0.1\varepsilon_0$. A stronger repulsion of $1.0\varepsilon_0$ is imposed on M_i–$\mathrm{ND}_{\mathrm{J}}^{(j)}$ interactions, for $i \neq j$, which notably affects the monomer distribution, lowering it to $g(r) < 1$. This is a manifestation of the Janus ND assembly at the bicontinuous interface, with one lobe positioned on one side and the other lobe on the opposite. The center of mass curve shows that these curves are exactly complementary.

Turning to the ND-NR RDFs in Fig. S4, we observe that the distribution of NDs around NRs, and *vice versa*, is nearly homogeneous. The curves for the various ND types are nearly identical, showing no influence of ND-monomer interactions on the ND-NR spatial distribution, and indicating independence from the chosen polymer matrix, as both matrices yield very similar results. ND_k/NR-BCPNCs exhibit a slight deviation from homogeneity due to their anisotropy, but the resulting curves still reflect a largely homogeneous distribution.

S4. POLYMER MEAN SQUARED DISPLACEMENT

TABLE S3: Diffusion coefficients ($\mathrm{nm}^2/\mathrm{ns}$) of the polymer's center of mass (COM) and of the monomers (MON). All the errors are under 0.003 $\mathrm{nm}^2/\mathrm{ns}$.

System	D_{COM}	D_{MON}
HP Melt	0.038	0.052
ND_1-HPNC	0.033	0.047
NR-HPNC	0.040	0.059
ND_1/NR-HPNC	0.032	0.045
BCP Melt	Not diff.	Not diff.
ND_1-BCPNC	Not diff.	Not diff.
NR-BCPNC	0.010	0.021
ND_1/NR-BCPNC	0.007	Not diff.

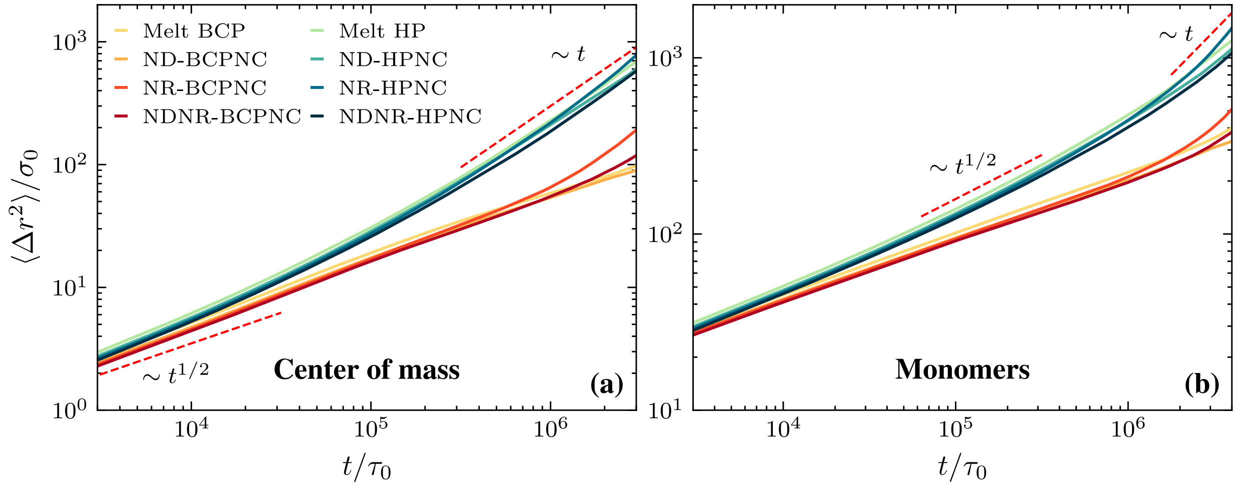

FIG. S5: Mean squared displacement of the polymer chain from the center of mass (left) and of the monomers (right) in the different systems. Two red dashed lines indicate the subdiffusive and diffusive tendencies.

S5. NON-GAUSSIAN PARAMETER

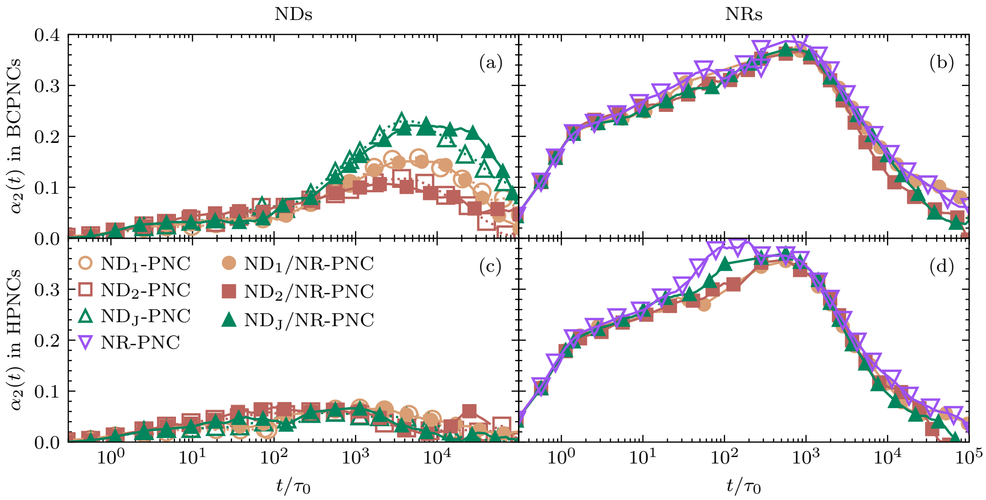

FIG. S6: Non-Gaussian parameter of NDs (left panels) and NRs (right panels) in BCPNCs (top row) and HPNCs (bottom row). ND$_k$-PNCs and NR-PNCs are depicted with empty symbols, while ND$_k$/NR-PNCs are shown with filled symbols, as indicated in the legend. Solid and dashed lines serve as visual guides.

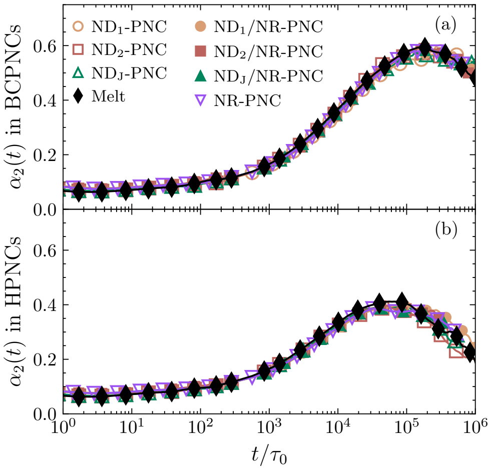

FIG. S7: Non-Gaussian parameter of monomers in BCPNCs (top panel) and HPNCs (bottom panel). ND$_k$-PNCs and NR-PNCs are represented by empty symbols, while ND$_k$/NR-PNCs are shown with filled symbols, as indicated in the legend. For comparison, the curve of pristine polymers is also included (represented by solid diamonds). Solid lines serve as visual guides.

S6. NANOCOMPOSITES UNDER SHEAR

To determine the value of viscosity at a specific shear rate, we employ NEMD simulations by applying shear to the top part of the simulation box. Initially, the polymer chains oppose this movement until a threshold is overcome. From that point onwards, the polymer chains align with the shear, facilitating the movement and thereby reducing the viscosity to a constant value that is maintained over time—see Fig. S8. A video showing the evolution of the PNCs under shear is available as a supplementary file titled `VideoShearing.mp4`.

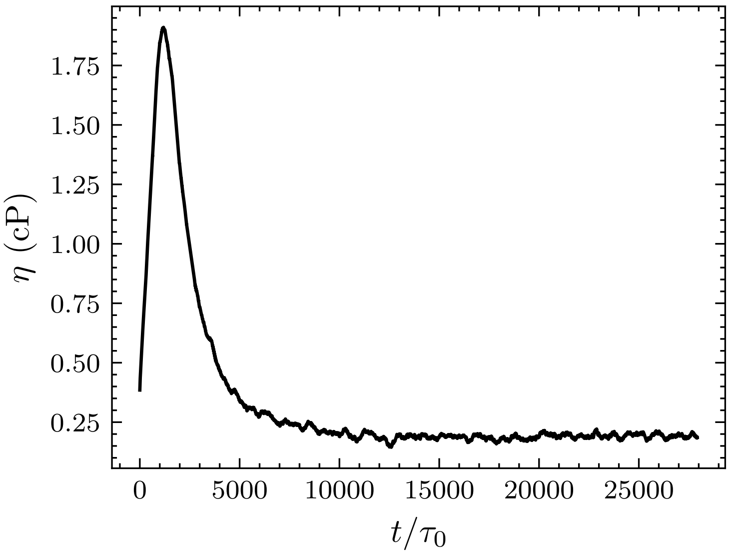

FIG. S8: Time evolution of the viscosity of a NR-BCP-PNC at an applied shear rate of $\dot{\gamma} = 4.3 \times 10^{-3}$ ps^{-1}, showing an initial peak in viscosity that later stabilizes.

S7. ZERO-SHEAR VISCOSITY WITH GREEN-KUBO

The zero-shear viscosity has been determined using the Green-Kubo formalism of integrating the autocorrelation functions of the off-diagonal components of the shear stress tensor. For this, we started from an equilibrated configuration and developed 150 ns simulations to test how the sampling affects the Green-Kubo integral, storing the pressure files each 2 fs. Doing so, we obtain a smooth and reliable curve of the pressure fluctuations, but it quickly becomes too detailed to be integrated with a reasonable amount of computational resources. To overcome that problem, we trimmed the stress tensor which contained data for every 2 fs to 100 fs steps and to 500 fs steps, and then performed the Green-Kubo integral

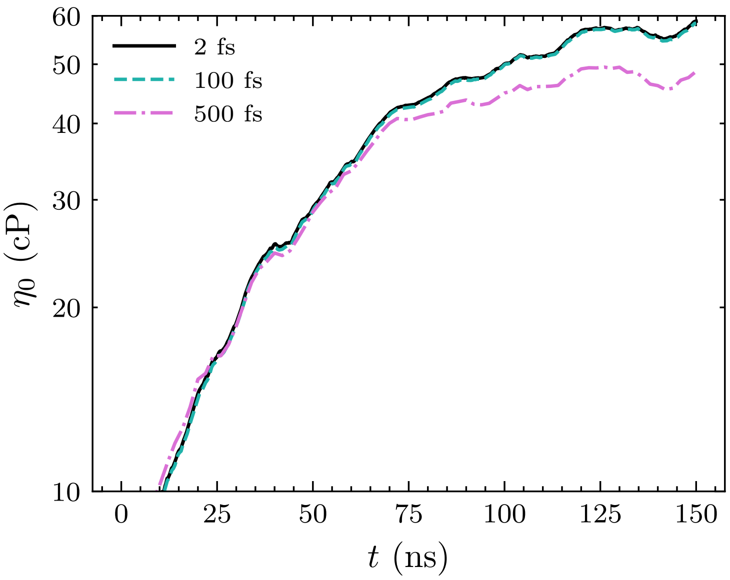

FIG. S9: Viscosity curves obtained using the Green-Kubo method for the HP melt system. Each curve corresponds to different sampling densities of the stress tensor, as indicated in the legend.

for comparison. We found out that for 100 fs the results are basically equivalent inside the resulting error bars, and that a skipping step of 500 fs turns out to be too large to recover the 2 fs statistics, see Fig. S9.

After this, we conducted 7 μs of equilibrium simulations with a 100 fs sampling interval to determine the viscosity of the studied PNCs. The average Green-Kubo results (planes XY, XZ and YZ) for the zero-shear viscosity are shown in Fig. S10. Using the same criterion for all systems, we performed the average calculation over the period from 2 to 7 μs. During this time, some curves have fully converged, while others still exhibit fluctuations, inevitably increasing our degree of uncertainty.

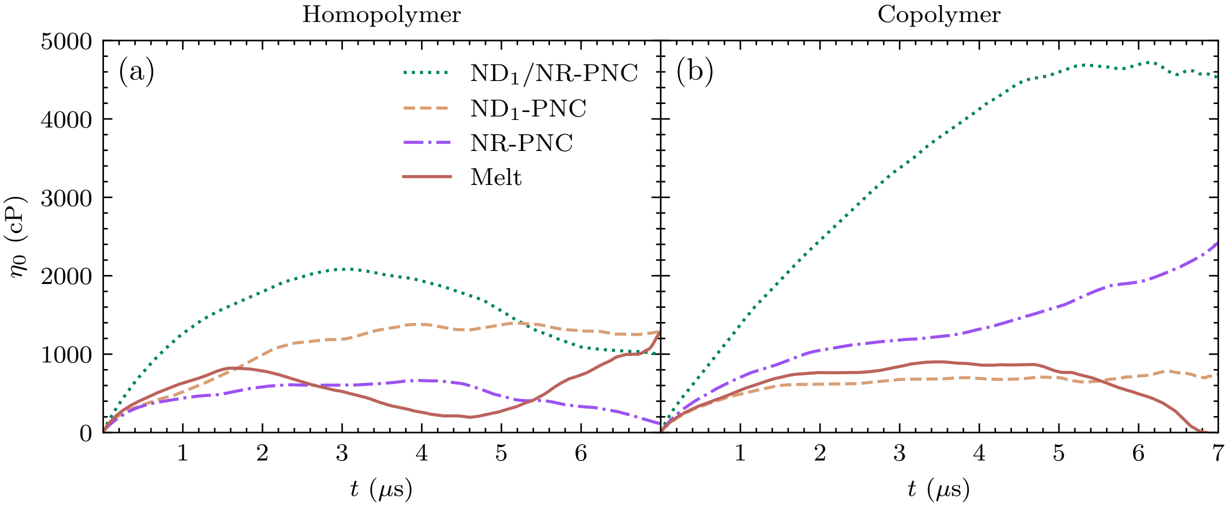

FIG. S10: Evolution of the average Green-Kubo integral with time. Systems with a homopolymer matrices are shown on the left, and systems with copolymer matrices are shown on the right.

REFERENCES

[1] R. Everaers, H. A. Karimi-Varzaneh, F. Fleck, N. Hojdis, and C. Svaneborg, “Kremer–Grest Models for Commodity Polymer Melts: Linking Theory, Experiment, and Simulation at the Kuhn Scale,” Macromolecules **53**, 1901–1916 (2020).

[2] J. J. Burgos-Mármol and A. Patti, “Molecular Dynamics of Janus Nanodimers Dispersed in Lamellar Phases of a Block Copolymer,” Polymers **13**, 1524 (2021).

[3] G. S. Grest and K. Kremer, “Molecular dynamics simulation for polymers in the presence of a heat bath,” Physical Review A **33**, 3628 (1986).

[4] K. Kremer and G. S. Grest, “Dynamics of entangled linear polymer melts: A molecular-dynamics simulation,” The Journal of Chemical Physics **92**, 5057–5086 (1990).